The method of biharmonic pumping in investigations of the electronic spectra of quantum-well structures

L. N. Vereshchagina and A. N. Zherikhin

Research Center for Technological Lasers, Russian Academy of Sciences, 140700 Shatura, Moscow Province, Russia

A. G. Kornienko, V. M. Petnikova, and V. V. Shuvalov

International Laser Center, M. V. Lomonosov Moscow State University, 119899 Moscow, Russia

(Submitted 18 July 1995)
Zh. Éksp. Teor. Fiz. **109**, 923–938 (March 1996)

A new method is proposed for investigating quantum-well structures based on optical Raman excitation and probing of allowed transitions in the renormalized spectrum of the electronic states. The method has been tested on ultrathin single-crystal PbTe films of thickness $L=6$, 18, and 30 nm. A strong dependence of the spectral position of the Raman electron resonances on L was found. The results of the experiment are interpreted in the framework of a model that takes into account the real band structure, electron–electron and electron–phonon interactions, and redistribution of the carriers through interband and intraband relaxation. A lower bound is obtained for the dephasing time of the interband polarization: $T_2 \geqslant 300$ fs in PbTe.
 [S1063-7761(96)01703-5]

1. INTRODUCTION

In recent years, there has been considerable interest in investigations of the electronic spectra $E_i(\mathbf{k})$ of ultrathin (of thickness $L_i=1-100$ nm) single-crystal films of various materials.[1] Here E is the energy of the carrier, $\mathbf{k}$ is its wave vector, and i is the band number. From investigations of metals and wide-gap semiconductors,[1–5] it became known that the electronic spectrum of such objects differs appreciably from the band structure of bulk samples, and the observed changes became known as the quantum size effect. It was found that if the sample thickness in some direction z is comparable with the electron de Broglie wavelength, then it is necessary to take into account size quantization of its quasimomentum in that direction, and $\hbar k_z=\pi\hbar s/L$, where $s=0,\ldots,s_{\max}$ is the quantum number. The changes in the spectrum are interpreted as splitting of the three-dimensional bands $E_i(\mathbf{k})$ into series of two-dimensional subbands $E_i(k_x,k_y,s)=E_i(\mathbf{k}_\perp,s)$, the total number of which is determined by the size and shape of the Brillouin zone; in the simplest case, for a cubic lattice with period a, the number is $s_{\max}\approx L/a$.

There are three main reasons for the interest in the quantum size effect. First, the development of microelectronics has made it necessary to use elements of the smallest sizes. Second, it was found that in this way materials with fundamentally new properties can be created. Finally, as we shall see, the quantum size effect is one of the few macroscopic manifestations of the fundamental quantum properties of matter.

Changes in electronic structure associated with the quantum size effect are both quantitative (renormalization of the band edges) and qualitative (splitting of the bands into series of two-dimensional subbands), and therefore variation of L usually leads to oscillations of the thermodynamic and transport parameters.[6,7] This effect was first found in thin bismuth films—from oscillations of the carrier mobility, the Hall constant, and the magnetoresistivity.[8] Somewhat later, size quantization was observed directly—in experiments on carrier tunneling through the potential barrier between two ultrathin films.[9] Subsequently, similar effects were studied in two-dimensional periodic structures with alternating thin films of different materials—superlattices and structures with even lower space dimension: quantum wires and quantum dots.[10] By now, a rather rich store of experimental material has been accumulated from investigation of the quantum size effect in wide-gap semiconductors,[2–5] and for this work one of the most effective approaches was proved to be the use of optical spectroscopy.[11] However, in most of the experiments done hitherto quantum-well structures based on GaAs have been used.[5] The number of studies that have been devoted to the quantum size effect in structures based on narrow-gap semiconductors is extremely small. The primary reason for this is that for the former it is possible to achieve single-photon excitation of transitions by means of radiation sources in the near infrared or visible range, whereas for the latter the experiments must be done in the intermediate or far infrared ranges. Although it is known that this problem can in principle be solved by using the methods of nonlinear spectroscopy with two-photon excitation and probing of transitions as in the method of biharmonic pumping,[12,13] such investigations have not yet been made. This is why the aim of the work reported here was to make a first experimental and theoretical investigation of manifestations of the quantum size effect in ultrathin single-crystal films of the narrow-gap semiconductor PbTe by the method of picosecond biharmonic pumping.

As with other methods of stationary four-photon spectroscopy, biharmonic pumping is used to study the dependence of the components of the nonlinear cubic susceptibility tensor on the frequency arguments. The data obtained on the spectral position, profile, and nature of the broadening of

 1063-7761/96/030497-09$10.00

both discrete lines and broad bands give information on the electronic and phonon spectra of the investigated material, electron–electron ($e-e$) and electron–phonon ($e-p$) coupling constants, relaxation times, etc. In biharmonic pumping, two electromagnetic waves with frequencies $\omega_{1,2}$ and wave vectors $\mathbf{k}_{1,2}$ "pump" the investigated medium. Through $e-e$ and $e-p$ interactions in the medium, there arise low-frequency electronic and phonon excitations at the difference frequency $\Delta=\omega_1-\omega_2$ with wave vector $\Delta\mathbf{K}=\mathbf{k}_1-\mathbf{k}_2$. The components of the biharmonic pumping themselves probe the resulting state and, being diffracted by the nonstationary grating "imprinted" in the sample, generate polarization waves at the Raman frequencies $\omega_3=2\omega_{1,2}-\omega_{2,1}$ with wave vectors $\mathbf{k}_3=2\mathbf{k}_{1,2}-\mathbf{k}_{2,1}$. It is this process—the self-diffraction of light—that makes it possible, by varying Δ, to investigate the spectrum of such excitations through the use of tunable lasers in the visible part of the spectrum. In an experiment, one usually determines the dependence of the self-diffraction efficiency η on Δ. It is this dependence that carries information on the frequencey dependence of the square of the modulus of the nonlinear cubic susceptibility $|\chi^{(3)}(\omega_3;\omega_{1,2}-\omega_{2,1},\omega_{1,2}|^2$. We recently successfully used such an approach to determine the parameters of the band gap in the state spectrum of superconducting Y–Ba–Cu–O samples.[13] Since all possible transitions in the Brillouin zone contribute to the nonlinear response to biharmonic pumping, it was to be expected that the quantum size effect would also be manifested in a displacement of single- and two-photon resonances and in a transformation of the dependence $\eta(\Delta)$. The position of the resonances will be determined by L and the conditions under which the experiment is set up, i.e., the temperature of the sample, the spectral range in which the measurements are made, etc.

There were numerous reasons why we chose ultrathin PbTe films to investigate the quantum size effect. First, it was found that by means of laser deposition it is possible to fabricate continuous single-crystal PbTe films with entirely suitable thicknesses $L=3-30$ nm (Ref. 14). Moreover, these films also were of high optical quality. Second, PbTe is a narrow-gap semiconductor with a band gap $E_g=0.32$ eV (Refs. 15–18) and has not hitherto been investigated by the methods of nonlinear spectroscopy. Third and last, in PbTe there are no optical phonon modes active in processes of the type of Raman scattering,[19] which should facilitate the analysis of the experimental data and made PbTe a convenient object for investigating precisely the electronic spectrum.

It is necessary to point out the very important role of a model that faithfully matches the experimental conditions and that is needed both to interpret all the data and to determine the values of the adjustable parameters, i.e., to extract spectroscopic information. For this, we adapted to the quantum-well case the model we had developed to calculate the nonlinear response to biharmonic pumping of semiconductors, metals, and superconductors.[12,20] However, for numerical modeling it was necessary to describe the electronic spectrum as accurately as possible. The required information was obtained by interpolating data on the band structure of bulk PbTe samples obtained for its symmetry axes by the pseudopotential method[21] and by solving model kinetic equations.

2. EXPERIMENT

In the course of the experiments, we investigated ultrathin PbTe films deposited on BaF_2 substrates by laser deposition. In the process of their preparation, a bulk target of a PbTe single crystal and a single-crystal substrate of orientation [111] and thickness 0.5 mm were placed in a vacuum chamber at a residual pressure of at most 10^{-7} Torr. A special method of mechanical and chemical polishing made it possible to reduce the scale of roughness of the working faces of the substrate to at most 2 nm. The distance from the substrate to the target was 5 cm. The substrate was placed on a heater kept at 250 °C. The target was evaporated by means of radiation from Lambda Physics LPX-203 pulsed KrF laser with energy density 1 J/cm^2. The pulse energy, the diameter of the irradiated surface, the distance to the substrate, and its temperature were carefully optimized, and this made it possible to eliminate more or less completely the formation of clusters.[14] The thicknesses of the fabricated films were measured using the Telystep profilometer with minimum height 0.5 nm of a detectable step. A continuous film with a thickness of two monolayers was deposited in 100 ± 10 laser pulses, and this made it possible to control L by the number of pulses. By this method, we succeeded in depositing continuous single-crystal PbTe films with thicknesses from 3 to 30 nm. An x-ray diffraction test of their quality showed that the admixture of orientations different from [100] did not exceed 1%. The samples were of optical quality and had a characteristic specular luster.

The arrangement of the spectroscopic complex was the traditional one for the method of biharmonic pumping and was essentialy identical to the one we described in Refs. 12 and 13. The master Q-switched picosecond YAG:Nd^{3+} laser based on dye No. 2681 in a polymer matrix was operated in the passive mode locking regime. After frequency doubling, its radiation was used for the phase-locked pumping of two independently tunable lasers based on the dye solution FN-70. The pulses of the dye laser (tuning range 590–645 nm, duration $\tau_p=20$ ps, peak power up to 50 kW, spectral width 1.5 cm^{-1}) were matched in time, and the beams were focused and directed at an angle of 7° onto the sample. The dimensions of the elongated spots produced by the beams on the film varied in the range 160–450 μm depending on the film thickness. The dye laser pulses were brought to a coincident point in frequency, time, and space by means of the correlation method, i.e., by maximizing of the efficiency of self-diffraction in single-crystal GaSe films of thickness 10–20 μm (Ref. 12).

In the course of the experiments, we measured $\eta(\Delta)$ for films of thickness $L=6$, 18, and 30 nm. Variation of Δ in the range 0–800 cm^{-1} was achieved by tuning the frequency of one of the dye lasers. As L was decreased, the energy density of the laser pulses was reduced by decreasing the degree of focusing and introducing additional calibrated neutral-density filters to ensure that the temperature of a film of any thickness remained unchanged. The detection system monitored the pulse energy at the fundamental frequency, at the

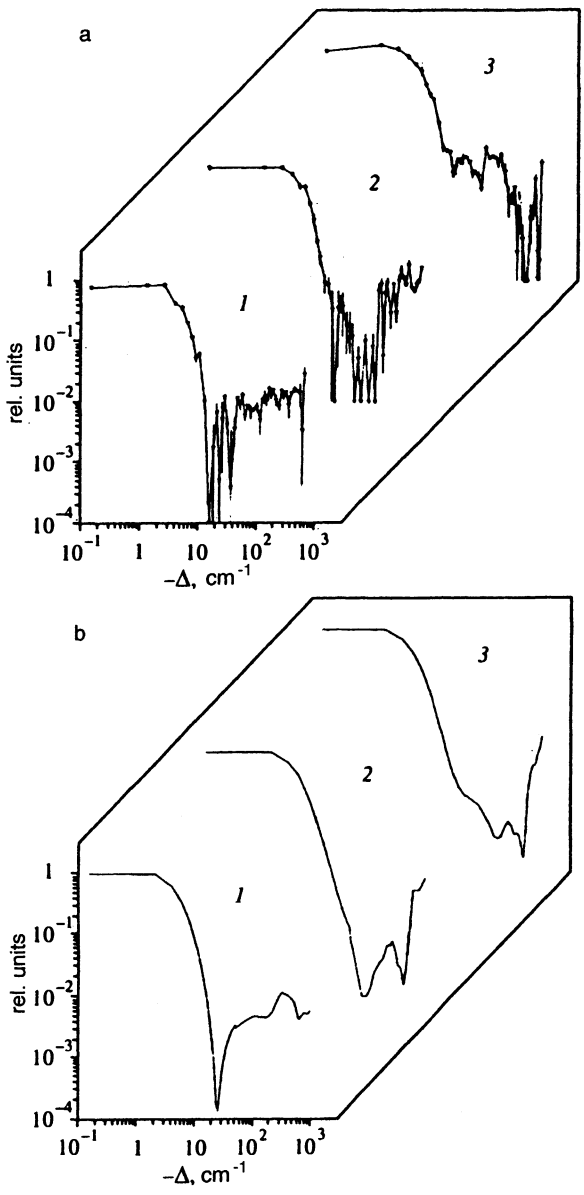

FIG. 1. Experimental (a) and theoretical (b) self-diffraction efficiency η as a function of frequency offset Δ of biharmonic pump components for PbTe films of thickness *1*) $L=6$ nm, *2*) $L=18$ nm, and *3*) $L=30$ nm.

frequency of the second harmonic, and at the frequencies of the dye laser and self-diffraction. The sensitivity in the radiation channel at the Raman frequency reached 10^{-16} J/pulse due to an efficient spatial filter system. The photodetector signals were digitized and analyzed on a computer. Control measurements showed that the level of the self-diffraction signal from the substrates without films was definitely below the instrumental sensitivity threshold.

Figure 1a shows the dependences $\eta(\Delta)$ obtained typically for samples of thickness $L=6$, 18, and 30 nm for the $\omega_4=2\omega_1-\omega_2$ process.[22] The initial temperature of the films was 300 K, and ω_1 was not changed and corresponded to the laser wavelength $\lambda_1=620.4$ nm. All the dependences are of the same kind and have two characteristic regions as functions of Δ: a narrow central peak at $\Delta<10$ cm^{-1} goes over smoothly into a broad wing at 10 cm$^{-1}<\Delta<800$ cm^{-1} with mean signal level η approximately equal to 10^{-2} of its maximum value at $\Delta=0$. The width of the central peak is of the order of twice the spectral width of the dye laser radiation. The wing is cut into by well-defined resonances, the positions of which change rapidly with L. There is a radical decrease of the resonance frequencies from the range 300 cm$^{-1}<\Delta<800$ cm^{-1} to the range 15 cm$^{-1}<\Delta<35$ cm^{-1} when L is reduced from 30 to 6 nm. All the resonances have a clear interference nature, and the change in their position on the Δ axis with change in L can be due only to manifestation of the quantum size effect. Since the optical phonon modes in PbTe are Raman inactive,[19] we attribute this series of maxima and minima to two-photon excitation of transitions in the electron subsystem. Although their positions do carry complete information about the renormalized electronic spectrum, it is not at all easy to extract it in "pure" form. The fact is that the condition of single-photon electron resonance is not satisfied at a single point but on some curve in the Brillouin zone that is the solution of the equation $E_i-E_j=\hbar\omega_{1,2}=$const. Since the frequency of the corresponding Raman resonance changes along this curve, the observed line is inhomogeneously broadened. Moreover, in the Brillouin zone of PbTe there are several regions in which a direct single-photon electron transition can take place, and the Raman resonance in them has different frequencies. This is equivalent to the presence in the nonlinear susceptibility of several interfering resonance components displaced in Δ. This is probably the reason for the very complicated structure of the electronic resonances observed in the experiment in the dependences $\eta(\Delta)$.

3. OVERALL STRUCTURE OF THE MODEL

The model of nonlinear response that we used to interpret the experimental data is analogous to the one employed in Ref. 20 to analyze the response of bulk samples. However, we introduced important corrections to take into account the specific features of the investigated object. As in Ref. 20, the structure of its state space H was reduced to the form

$$H=H_A\otimes H_R, \tag{1}$$

where the index A identifies the "active" variables that directly determine the nonlinear response, while R identifies the "reservoir" variables responsible for relaxation and noise. On the basis of the Liouville equation for the density matrix $\hat{\rho}$, we then calculated $\chi^{(3)}$. By averaging over the reservoir variables, we reduced the equation for the complete system in the space H to the equation

$$\frac{d\hat{\rho}_A}{dt}=\int_{-\infty}^{t}\hat{\Phi}(t,t')\hat{\rho}_A(t')dt' \tag{2}$$

for the active subsystem in the space H_A. Here $\hat{\rho}_A$ determines the equal-time distribution of the probabilities of the active variables, and $\hat{\Phi}$ is the operator that describes the evolution with allowance for all disturbances of the active subsystem. It was assumed that at the initial time $t_0=-\infty$ this subsystem and the reservoir are statistically independent and $\hat{\rho}=\hat{\rho}_A\times\hat{\rho}_R$. The solution of (2) was represented in the form

$$\hat{\rho}_A(t)=\tilde{S}(t,t_0)\hat{\rho}_A(t_0), \tag{3}$$

where the superoperator

$$\tilde{S}(t,t_0)=\mathrm{Tr}_R\hat{U}(t,t_0)\oplus\hat{\rho}_R\hat{U}^{-1}(t,t_0) \tag{4}$$

describes the transition probability distribution for the active variables, and $\oplus$ is the symbol for substitution of the transformed density matrix $\hat{\rho}_A(t_0)$. The evolution operator $\hat{U}$ was expressed in the standard manner[20] in terms of the total Hamiltonian

$$\hat{H}=\hat{H}_C+\hat{H}_I, \quad \hat{H}_C=\hat{H}_A+\hat{H}_F+\hat{H}_R, \tag{5}$$

where $\hat{H}_{A,I,F,R}$ described the active subsystem, its interaction with the external field and noise, and the reservoir. The solution

$$\hat{\rho}_A^{(3)}(t)=\hat{\rho}^{(\alpha)}(t)+\hat{\rho}^{(\beta)}(t) \tag{6}$$

of Eq. (2) was found by successive approximation in the third order of perturbation theory in $\hat{H}_I$ with allowance for terms corresponding to processes of the form $\omega_4=\omega_i-\omega_j+\omega_k$ $(i,j,k=1,2,3)$. Here

$$\hat{\rho}^{(\alpha)}=\frac{i}{\hbar^3}\int_{t_0}^{t}dt_3\int_{t_0}^{t_3}dt_2\int_{t_0}^{t}dt_1\hat{U}_A(t-t_1)\{\tilde{S}_\alpha(t,t_1;t_2,t_3)\times[\hat{H}_1^{(-)}(t_1)\hat{H}_1^{(+)}(t_2)]\}\hat{U}_A^{-1}(t_3-t_2)\hat{H}_1^{(-)}(t_3), \tag{7}$$

$$\hat{\rho}^{(\beta)}=\frac{i}{\hbar^3}\int_{t_0}^{t}dt_3\int_{t_0}^{t_3}dt_2\int_{t_0}^{t_2}dt_1\hat{U}_A(t-t_3)\{\tilde{S}_\beta(t,t_3;t_2,t_1)\times[\hat{H}_1^{(-)}(t_3)\hat{H}_1^{(+)}(t_2)]\}\hat{U}_A(t_2-t_1)\hat{H}_1^{(-)}(t_1),$$

$\hat{U}_A(t)$ is the evolution operator in the space H_A,

$$\hat{H}_I=\hat{H}_I^{(+)}+\hat{H}_I^{(-)}=H_I^{(+)}\hat{a}^+(\mathbf{K}_f)\hat{a}(\mathbf{K}_i)+H_I^{(-)}\hat{a}^+(\mathbf{K}_i)\hat{a}(\mathbf{K}_f), \tag{8}$$

and $H_I^{(\pm)}$ are the Hermitian-conjugate matrix elements of the operators $\hat{H}_I^{(\pm)}$. The bilinear combinations of the operators of creation $\hat{a}^+$ and annihilation $\hat{a}$ describe the electron transition between states with wave vectors $\mathbf{K}_f$ and $\mathbf{K}_i$. The superoperators

$$\tilde{S}_\alpha(t,t_1;t_2,t_3)=\mathrm{Tr}_R\hat{U}_F(t,t_1)\oplus\hat{\rho}_R\hat{U}_F^{(-1)}(t_3,t_2),$$
$$\tilde{S}_\beta(t,t_3;t_2,t_1)=\mathrm{Tr}_R\hat{U}_F(t,t_3)\oplus\hat{U}_F(t_2,t_1)\hat{\rho}_R \tag{9}$$

define a transformation analogous to (3). The unitary operator

$$\hat{U}_F(t,t')=\hat{U}_R^{-1}(t'-t_0)T\times\exp\left\{-\frac{i}{\hbar}\int_0^{t-t'}\hat{H}_F(s)ds\right\}\hat{U}_R(t'-t_0) \tag{10}$$

takes into account the interaction of the active subsystem and the reservoir. Here $\hat{U}_R$ is the evolution operator of the reservoir, T is the time-ordering symbol, and $\hat{H}_F(s)$ is written down in the interaction representation with the unperturbed Hamiltonian $\hat{H}_A+\hat{H}_R$.

In the dipole approximation with allowance for the conservation of momentum when a photon with wave vector $\mathbf{k}_j$ is absorbed and emitted

$$H_I^{(\pm)}=-\frac{1}{2}V^{-1}\mathbf{d}^{(\pm)}(k_j)\mathbf{E}_j^{(\mp)}\exp(\pm i\omega_j t)P_V(\mathbf{K}_f-\mathbf{K}_i-\mathbf{k}_j), \tag{11}$$

and the calculation reduces to averaging the dipole-moment operator $\hat{\mathbf{d}}$ over the final state using (7). Here the indices $\pm$ correspond to the electron transitions $\mathbf{K}_f\leftrightarrow\mathbf{K}_i$, V is the volume of the unit cell, $\mathbf{d}^{(\pm)}(\mathbf{k}_j)$ are the off-diagonal matrix elements of $\hat{\mathbf{d}}$, and $\mathbf{E}_j^{(\pm)}=[\mathbf{E}_j^{(\mp)}]^*$ is the complex amplitude of the field with frequency ω_j. The Fourier transform P_V of the projection operator $\hat{P}_V$ onto the volume reflects the momentum conservation law, and for an infinite sample $P_V=\delta(\mathbf{K}_f-\mathbf{K}_i-\mathbf{k}_j)$. Thus, "imprinting" of an interference grating by the components of the biharmonic pumping with $\mathbf{k}_1\neq\mathbf{k}_2$ is possible only through scattering processes with transfer by an active electron of the momentum difference $\Delta\mathbf{K}=\mathbf{k}_1-\mathbf{k}_2$ to the electrons and phonons of the reservoir. The corresponding processes were described by the interaction Hamiltonians

$$\hat{H}_{FE}=\int d\mathbf{K}_{RE}\int d\Delta\mathbf{K}_{RE}A_E(\Delta\mathbf{K}_{RE})\hat{a}^+(\mathbf{K}_{RE})\times\exp[i\Delta\mathbf{K}_{RE}(\hat{\mathbf{Q}}_{RE}-\hat{\mathbf{Q}}_{AE})]\hat{a}(\mathbf{K}_{RE})+\mathrm{h.c.},$$
$$\hat{H}_{FP}=\sum_\lambda\int d\mathbf{K}_{RP}\{A_P^\lambda(\mathbf{K}_{RP})\hat{b}_\lambda(\mathbf{K}_{RP})\exp(i\mathbf{K}_{RP}\hat{\mathbf{Q}}_{AE})+\mathrm{h.c.} \tag{12}$$

Here $A_{E,P}$ are the $e-e$ and $e-p$ coupling constants, and $\hat{\mathbf{Q}}_{RE,AE}$ are the coordinate operators of a noise electron and an active electron. The creation (annihilation) operators $\hat{a}^+$ $(\hat{a})$ and $\hat{b}_\lambda^+$ $(\hat{b}_\lambda)$ are for the electron and phonon reservoirs with momenta $\mathbf{K}_{RE}$ and $\mathbf{K}_{RP}$, and integration is over the entire Brillouin zone.

More specifically, the operator of the intrinsic evolution in (7) was written in the form

$$\hat{U}_A(t)=\exp(-i\Delta\omega_{AE}t), \tag{13}$$

where $\hbar\Delta\omega_{AE}=E(\mathbf{K}_f)-E(\mathbf{K}_i)$ is the difference between the energies of the final and initial states determined by the band structure. In averaging over the reservoir variables in (9), we retained terms containing the superoperator

$$\tilde{T}(\Delta\mathbf{K})=\exp(-i\Delta\mathbf{K}\hat{\mathbf{Q}}_{AE})\oplus\exp(-i\Delta\mathbf{K}\hat{\mathbf{Q}}_{AE}) \tag{14}$$

of momentum shift of an active electron by the amount $\Delta\mathbf{K}$ needed for self-diffraction. It was assumed that the contribution of many-particle processes to the resonance part of the response reduces to a "pure" phase relaxation, i.e., in (9) we separated explicitly the coherent, c, and relaxation, r, components:

$$\tilde{S}_{\alpha,\beta}=\tilde{S}^{(c)}_{\alpha,\beta}\tilde{S}^{(r)}_{\alpha,\beta}. \tag{15}$$

The former was approximated by the lowest-order terms of the expansion (9) in the $e-e$ and $e-p$ coupling constants and for processes of $e-e$ type:

$$\tilde{S}^{(c)}_{\alpha}=\hbar^{-2}\int d\mathbf{K}_{RE}\int_0^{t-t_1}ds_1\int_0^{t_2-t_3}ds_2 n(\mathbf{K}_{RE}-\Delta\mathbf{K})$$
$$\times[1-n(\mathbf{K}_{RE})]\exp[i\Omega_{RE}(t_1-t_3+s_1-s_2)],$$
$$\tilde{S}^{(c)}_{\beta}=\hbar^{-2}\int d\mathbf{K}_{RE}\int_0^{t-t_3}ds_1\int_0^{t_2-t_1}ds_2 n(\mathbf{K}_{RE}) \tag{16}$$
$$\times[1-n(\mathbf{K}_{RE}-\Delta\mathbf{K})]\exp[i\Omega_{RE}(t_3-t_1+s_1-s_2)].$$

Here the transition frequencies Ω_{RE} are determined by the band structure, $\hbar\Omega_{RE}=E(\mathbf{K}_{RE})-E(\mathbf{K}_{RE}-\Delta\mathbf{K})$, and n are the occupancies of the electron states of the reservoir $\mathbf{K}_{RE}$ and $(\mathbf{K}_{RE}-\Delta\mathbf{k})$. The relaxation component in (15) is determined by the many-particle scattering processes for which $\Delta\mathbf{K}\equiv 0$. The corresponding phase relaxation process was assumed to be a Markov process:

$$\tilde{S}^{(r)}_{\alpha}=\exp[-\Gamma(t-t_1-t_2+t_3)],$$
$$\tilde{S}^{(r)}_{\beta}=\exp[-\Gamma(t-t_1+t_2-t_3)]. \tag{17}$$

As will be clear from what follows, the corrections to n and the dependence of the relaxation rate Γ in (17) on the position in the Brillouin zone were taken into account phenomenologically.

4. PARTICULARIZATION OF THE MODEL

In the nonlinear susceptibility $\chi^{(3)}$, three additive components were identified: the resonant electron component $\chi^{(3)}_{ee}$, associated with momentum transfer to the electron subsystem of the reservoir by single-particle scattering, the resonant phonon component $\chi^{(3)}_{ep}$ due to analogous processes of $e-p$ type, and the nonresonant component $\chi^{(3)}_{nr}$, which includes the contributions of all many-particle processes of both $e-e$ and $e-p$ type. The first of these was found by integrating (7) with allowance for (15)–(17):

$$\chi^{(3)}_{ee}\propto(\delta k_z)^3 P_0\{K_+P_++K_-P_-\}, \tag{18}$$

where

$$P_0=\sum_{i,s,i',s'}\int\frac{n_i(\mathbf{k}_\perp,s)[1-n_{i'}(\mathbf{k}_\perp,s')]}{\{\omega_1-\Omega_{i,s,i',s'}(\mathbf{k}_\perp)+i\Gamma_{i,s,i',s'}(\mathbf{k}_\perp)\}^2}d\mathbf{k}_\perp, \tag{19}$$

$$P_\pm=\sum_{i,s,i',s'}\int\times\frac{n_i(\mathbf{k}_\perp,s)[1-n_{i'}(\mathbf{k}_\perp,s')]}{\{\omega_1\pm\Delta-\Omega_{i,s,i',s'}(\mathbf{k}_\perp)\pm i\Gamma_{i,s,i',s'}(\mathbf{k}_\perp)\}^2}d\mathbf{k}_\perp, \tag{20}$$

$$K_\pm=\sum_{i,s,i',s'}\int\times\frac{n_i(\mathbf{k}_\perp,s)[1-n_{i'}(\mathbf{k}_\perp,s')]}{\{\pm\Delta-\Omega_{i,s,i',s'}(\mathbf{k}_\perp)\pm i\Gamma_{i,s,i',s'}(\mathbf{k}_\perp)\}}d\mathbf{k}_\perp. \tag{21}$$

Here s and s' are the numbers of the two-dimensional subbands of bands i and i'. Thus, (19)–(21) take into account splitting of the band structure into a system of two-dimensional subbands. The frequencies of the electron transitions $(i,s,\mathbf{k}_\perp)\rightarrow(i',s',\mathbf{k}_\perp)$ are defined as

$$\Omega_{i,s,i',s'}(\mathbf{k}_\perp)=[E_{i'}(\mathbf{k}_\perp,s')-E_i(\mathbf{k}_\perp,s)]/\hbar,$$

and $\Gamma_{i,s,i',s'}(\mathbf{k}_\perp)$ are the reciprocal relaxation times of the corresponding transitions. The factor $\delta k_z=a/L$ in (18) ensures a common normalization of the response for films of different thickness by conservation of the total number of states in the Brillouin zone. In what follows, the electron transitions in (19)–(21) were assumed to be direct, and this led to conservation of the projection k_z and to the selection rule $s=s'$. The terms of the sums (19)–(21) correspond to allowed transitions in the renormalized electron spectrum and, in principle, can occur in (18) with different weights. In the general case, their relative contribution must be determined by the overlap integral of the wave functions of the corresponding pair of states. In what follows, this relative contribution was assumed to be the same for all allowed transitions.

4.1. Approximation of the band structure of PbTe

For the numerical calculation of $\chi^{(3)}_{ee}$ (18), it was necessary to describe as accurately as possible the electronic spectrum $E_i(\mathbf{k}_\perp,s)$ of the investigated samples and to determine the frequencies of all possible transitions $\Omega_{i,s,i',s'}(\mathbf{k}_\perp)$. To do this, we approximated numerically in the complete Brillouin zone the dependences $E_i(\mathbf{k})$ obtained for the symmetry axes of bulk PbTe samples by the pseudopotential method.[21] We took into account the first three bands of the valence band ($i=1,\ldots,3$) and the two lowest bands of the conduction band ($i=4,5$). For their approximation by a system of polynomials, two algorithms were used—the method of least squares and an algorithm that minimizes the gradient of the approximating function. Their relative weights were chosen in such a way that the first algorithm ensured an accuracy of approximation of the data of Ref. 21 no worse than 0.03 eV, and the second algorithm made it possible to avoid the appearance of "parasitic" extrema. Then, taking into account the condition of size quantization in a potential well with infinitely high walls, we calculated the dependences $E_i(\mathbf{k}_\perp,s)$ for the quantum-well samples.

4.2. Kinetics of free carriers

The functional dependence needed to calculate the relaxation rates $\Gamma_{i,s,i',s'}(\mathbf{k}_\perp)$ was modeled on the basis of simple physical arguments. Characteristic times of the following relaxation processes were introduced.

1. Intraband occupancy relaxation (T_3), which described thermalization of the valence band or the conduction

band as a whole. In what follows, it was assumed that $T_3=1$ ps, corresponding to the data of the experiment of Ref. 23.

2. Intrasubband occupancy relaxation (T_3'), which described the thermalization of carriers within one subband. It was assumed that this process takes place on the time scale $T_3' \sim 100-1000$ fs and that its rate depends on experimental conditions (free carrier concentration, temperature, etc.).

3. Carrier recombination (T_1). Usually, the values of T_1 lie in the nanosecond range.[24] In what follows, it was assumed that $T_1 \gg \tau_p$, and the contribution of recombination processes was ignored.

4. Decay of interband polarization (transverse relaxation) (T_2). All the processes listed above lead to transverse relaxation, and the corresponding time scale is the fastest of them. Thus, $T_2 \sim T_3' \sim 100-1000$ fs.

In the modeling, it was assumed that at each point of the Brillouin zone $\Gamma_{i,s,i',s'}(\mathbf{k}_\perp) \sim 1/T_2$ and that the relaxation rate contains two components. The first is determined by the concentration N of free carriers and by the relative velocity v_{rel} of colliding particles:

$$\Gamma^{(\alpha)}=\Gamma_0^{(\alpha)} N v_{\text{rel}}, \tag{22}$$

where $v_{\text{rel}}=\sqrt{v_0^2+\overline{v_R^2}}$, and $\Gamma_0^{(\alpha)}$ is an adjustable parameter of the model. The velocity v_0 of an active electron was assumed to be a local property of its position in the Brillouin zone, while the velocity v_R of a reservoir electron was averaged over the conduction band.

For ultrathin films containing a small number of atomic layers (about 10 for $L=6$ nm), the fact that the potential well is not rectangular leads to random phase distortions $e^{i\delta\varphi}$ of the electron wave function. Averaging these also effectively broadens the electronic transition:

$$\Gamma^{(\beta)}=\Gamma_0^{(\beta)} e^{W}. \tag{23}$$

Here $\Gamma_0^{(\beta)}$ is an adjustable parameter, and $W \sim \overline{(\delta\varphi)^2}$ is the Debye–Waller factor.[25] Under the assumption that these distortions become significant ($\delta\varphi \approx 1$) when the thickness of the "surface" layer of the film is comparable with the spatial period of the wave function in the direction of the size quantization, we obtain $\delta\varphi \propto s/L$. From this we obtain $W=(L_0/L)^2 s^2$, where the parameter L_0 determines the numbers of subbands that make a significant contribution to the response. In what follows, we assumed that $L_0=6$ nm.

The mechanisms (22) and (23) of broadening of the Lorentz factors in (19)–(21) were taken into account additively. Both terms increase with increasing s. Thus, in the method of biharmonic pumping, as in other methods of investigating the quantum size effect,[1,6] the contribution of the subbands with the lowest numbers is "emphasized."

This model makes it possible to go over to a limited number of adjustable parameters $\Gamma_0^{(\alpha)}$, $\Gamma_0^{(\beta)}$, and L_0, which describe the relaxation kinetics, while nevertheless maintaining locality of the description through explicit allowance for the dependences of the rates of the corresponding processes on $(i,s,\mathbf{k}_\perp)$. Approximate values in the range $\Gamma_0^{(\alpha)}=10^{-12}-10^{-13}$ cm^2 were obtained from the estimates for $T_2 \sim T_3' \sim 100-1000$ fs in massive semiconductor samples.[12,18] In the estimate $\Gamma_0^{(\beta)}=10^{12}-10^{13}$ sec^{-1}, it was assumed that for a film of thickness $L=6$ nm and $s=1$ the two broadening mechanisms make equal contributions.

4.3. Allowance for "hole burning"

In the model (19)–(21), the occupancies are given by the Fermi distribution, and at $\Theta \sim 10^3$ K for the Raman transitions ($i,i'=1-3$ or $i,i'=4,5$) $n_i(\mathbf{k}_\perp,s)[1-n_{i'}(\mathbf{k}_\perp,s')] \approx 0$. Therefore, even small corrections to the equilibrium values $n_i(\mathbf{k}_\perp,s)=n_i^0(\mathbf{k}_\perp,s)$ resulting from the effect of the light field at frequencies ω_1 and ω_2 (the so-called saturation effect) can significantly change the ratios of the contributions of the individual resonances to the total response. To calculate these corrections, we used the modified density matrix approach for an effective two-level system.[26] The corrections were obtained under the assumption of rapid relaxation of the off-diagonal elements of the density matrix by solving the kinetic equations for $n_i(\mathbf{k}_\perp,s)$:

$$\begin{aligned}\frac{\partial}{\partial t}[N\varphi_{is} f_i(\mathbf{k}_\perp,s)] &= -\left|\frac{\mathbf{dE}}{\hbar}\right|^2 \sum_{i',s'} \sum_{m=1,2} \frac{2\Gamma_2}{(\omega_m-\Omega_{i,s,i',s'}(\mathbf{k}_\perp))^2+\Gamma_2^2} \\ &\times N\varphi_{is} f_i(\mathbf{k}_\perp,s) - \frac{N-N^0}{T_1}\varphi_{is} f_i(\mathbf{k}_\perp,s) \\ &- N\frac{\varphi_{is}-\varphi_{is}^0}{T_3} f_i(\mathbf{k}_\perp,s) - N\varphi_{is}\frac{f_i(\mathbf{k}_\perp,s)-f_i^0(\mathbf{k}_\perp,s)}{T_3'}.\end{aligned} \tag{24}$$

Here the subscripts (i,s) and (i',s') identify the subbands of the valence band and conduction band; $N=\Sigma_{i,s}\int n_i(\mathbf{k}_\perp,s)d\mathbf{k}_\perp$ is the total number of electrons in the valence band; the functions $\varphi_{i,s}=\int n_i(\mathbf{k}_\perp,s)d\mathbf{k}_\perp / \Sigma_{i,s}\int n_i(\mathbf{k}_\perp,s)d\mathbf{k}_\perp$ and $f_i(\mathbf{k}_\perp,s)=n_i(\mathbf{k}_\perp,s)/\int n_i(\mathbf{k}_\perp,s)d\mathbf{k}_\perp$ describe their distribution by subband and within each subband. Equation (24) is written down for equal amplitudes of the biharmonic pumping components: $\mathbf{E}(\omega_1)=\mathbf{E}(\omega_2)=\mathbf{E}$; N^0, φ_{is}^0, and $f_i^0(\mathbf{k}_\perp,s)$ correspond to the Fermi distribution, and $\Sigma_{i',s'}$ includes subbands to which transitions are allowed ($s=s'$). Under the assumptions of slow recombination ($T_1=\infty$), relative smallness of the corrections $\Delta N=N^0-N$, $\Delta\varphi_{is}=\varphi_{is}^0-\varphi_{is}$ and $\Delta f_i(\mathbf{k}_\perp,s)=f_i^0(\mathbf{k}_\perp,s)-f_i(\mathbf{k}_\perp,s)$, and for $T_3, T_3' \ll \tau_p$ we have[23]

$$n_i(\mathbf{k}_\perp,s)=n_i^0(\mathbf{k}_\perp,s)[1-\delta n_i(\mathbf{k}_\perp,s)], \tag{25}$$

where

$$\delta n_i(\mathbf{k}_\perp,s)=\left|\frac{\mathbf{dE}}{\hbar}\right|^2\left\{\tau_p\sum_{i,s} I_i(\mathbf{k}_\perp,s)d\mathbf{k}_\perp - T_3\frac{\int I_i(\mathbf{k}_\perp,s)d\mathbf{k}_\perp}{\varphi_{is}^0} - T_3'\frac{\Sigma_{i,s} I_i(\mathbf{k}_\perp,s)}{f_i^0(\mathbf{k}_\perp,s)}\right\}, \tag{26}$$

$$I_i(\mathbf{k}_\perp,s)=\sum_{i',s'}\sum_{m=1,2}\frac{2\Gamma_2}{(\omega_m-\Omega_{i,s,i',s'}(\mathbf{k}_\perp))^2+\Gamma_2^2} \times \varphi_{is}^0 f_i^0(\mathbf{k}_\perp,s). \tag{27}$$

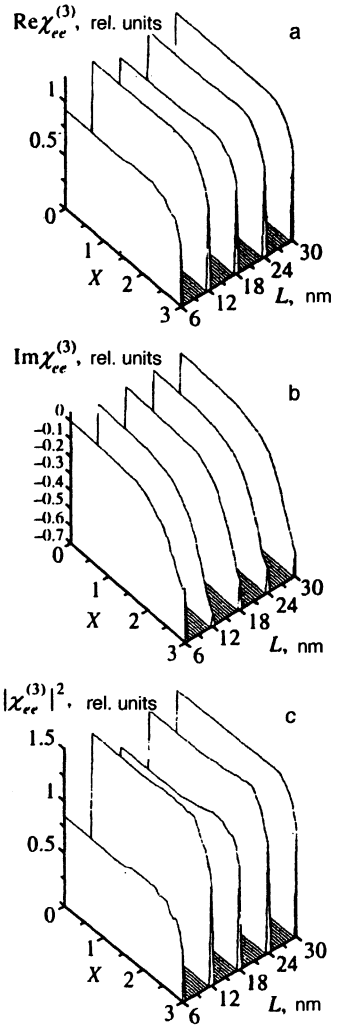

FIG. 2. Calculated resonant electronic susceptibility $\chi_{ee}^{(3)}(\Delta)$. $X=\log(-\Delta, \text{cm}^{-1})$, $T_2=100$ fs, $S=0$. a) Real part; b) imaginary part; c) squared amplitude.

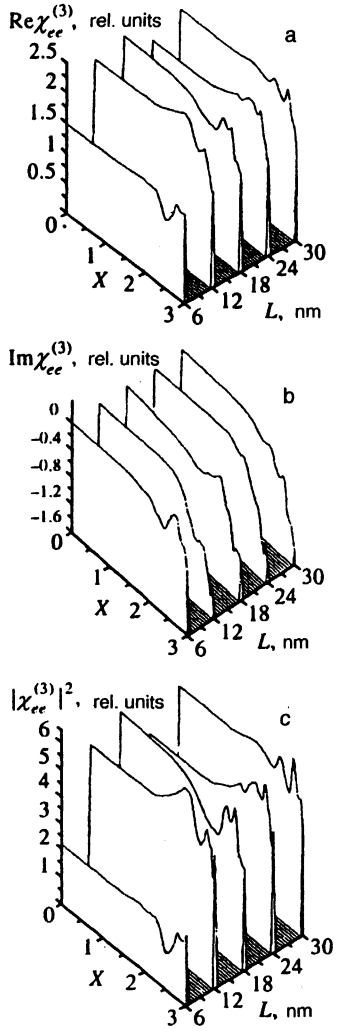

FIG. 3. Calculated resonant electronic susceptibility $\chi_{ee}^{(3)}(\Delta)$. $X=\log(-\Delta, \text{cm}^{-1})$, $T_2=300$ fs, $S=0$. a) Real part; b) imaginary part; c) squared amplitude.

As our subsequent calculation showed, allowance for even weak redistribution of the carriers ("hole burning" in the distribution function) significantly reinforces the contributions of two-photon transitions with the participation of subbands that are depleted or occupied by the light field . In what follows, field-induced carrier redistribution (25) will be be characterized by the degree of saturation S, which is defined as the maximum relative occupancy change in the Brillouin zone.

5. NUMERICAL RESULTS

In the model described above, we made a numerical calculation of the nonlinear response of ultrathin PbTe films of thicknesses 6–30 nm for different values of the adjustable parameters. We calculated $\chi_{ee}^{(3)}$ on the basis of (18) using the approximation of the real band structure of PbTe with allowance for the broadening mechanisms (22) and (23) and "hole burning" (25). The temperature of the electronic subsystem of the sample, heated by the picosecond pulse, was taken to be 1000 K (Ref. 12).

Figures 2 and 3 show the calculated dependences $\chi_{ee}^{(3)}$ for $T_2=100$ and 300 fs and $S=0$. The calculation showed that the nature of the dependences changes radically when T_2 is changed and that the interference resonances at $\Delta\geqslant 100$ cm^{-1} that we observed experimentally appear only when $T_2\geqslant 150$ fs. This enabled us to place a lower bound on the relaxation time of the interband polarization:

$$T_2\geqslant 300 \text{ fs}. \tag{28}$$

It follows from the previous section that the same bound holds for the intrasubband relaxation time T_3'. For $T_2=100$ fs (Fig. 2), one can clearly see how with increasing L the response of the quantum-well films converges to the limit—the response of the bulk sample. For $T_2=300$ fs (Fig. 3), this convergence does not occur all the way up to $L=30$ nm. Thus, under the conditions of our experiment the quantum size effect did indeed play a decisive role in the formation of the nonlinear response.

The transformation of $\chi_{ee}^{(3)}$ when T_2 is changed is illustrated by Fig. 4. For $T_2\geqslant 150$ fs, we see characteristic oscillations at frequencies $\Delta\geqslant 200$–300 cm^{-1}. Their relative amplitude increases with increasing T_2, while the spectral

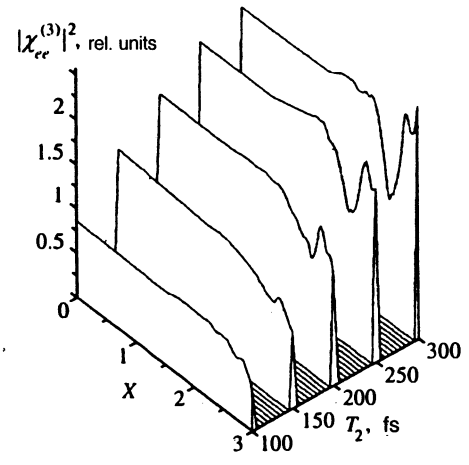

FIG. 4. Calculated $|\chi_{ee}^{(3)}(\Delta)|^2$ at various values of the transverse relaxation time T_2. a) Real part; b) imaginary part; c) squared amplitude. $X=\log(-\Delta, \text{cm}^{-1})$, $L=6$ nm, $S=0$.

position hardly changes. The variation of $\chi_{ee}^{(3)}$ with increasing S is shown in Fig. 5. The nonlinear response was found to be extremely sensitive to the redistribution of the carriers induced by the light field. Thus, increase of S from 0 to 1% leads to a growth of $|\chi_{ee}^{(3)}|^2$ by two orders of magnitude. In the case of a further increase in the degree of saturation, $|\chi_{ee}^{(3)}|^2$ depends quadratically on S, while the nature of the dispersion dependence and the relative amplitude of the oscillations in the region $\Delta \geqslant 200$–300 cm^{-1} remain essentially unchanged (Fig. 5).

On the basis of the estimate (28) and the numerical calculation of $\chi_{ee}^{(3)}$, we made an approximation of the experimental data (Fig. 1). The total nonlinear susceptibility was sought in the form

$$\chi^{(3)}=\chi_{ee}^{(3)}+\chi_{ep}^{(3)}+\chi_{nr}^{(3)}, \tag{29}$$

where the meaning of the components $\chi_{ep}^{(3)}$ and $\chi_{nr}^{(3)}$ was described in the previous section. The qualitatively different dependence of the components of (29) on Δ makes it possible to use the different sections of the experimental curves

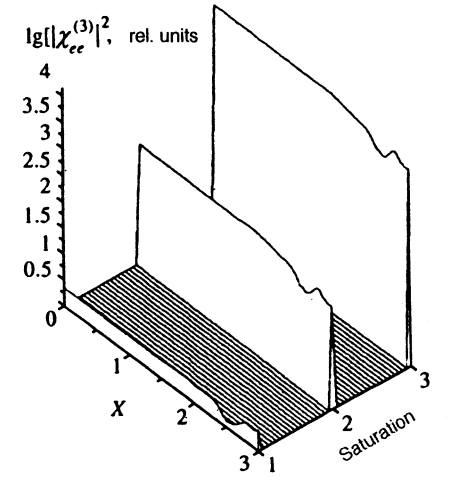

FIG. 5. Calculated $|\chi_{ee}^{(3)}(\Delta)|^2$ at various values of the saturation S. $X=\log(-\Delta, \text{cm}^{-1})$, $L=6$ nm, $S=0\%$ (*1*), $S=1\%$ (2), $S=10\%$ (3).

(Fig. 3a) to find the values of the adjustable parameters more accurately. Thus, in the region of the central peak ($\Delta<10$ cm^{-1}), the data of the experiment can be well approximated by the quadratic Lorentzian profile

$$\chi_{ac}/(\Delta-i\Gamma_{ac})^2, \tag{30}$$

for which the spectral width Γ_{ac} is approximately twice the width of the spectrum of the dye laser pulses. This is typical of a process whose rate is appreciably smaller than the spectral width of the components of the biharmonic pumping. It is natural to attribute the appearance of this peak to excitation of acoustic phonons and thermal nonlinearity. For PbTe, the contribution (30) completely describes $\chi_{ep}^{(3)}$, since two-photon excitation of optical phonons is forbidden in it. The complex amplitude $\chi_{ac}=\chi_{ac}^0 e^{i\Psi_{ac}}$ of this component was one of the adjustable parameters of our model. It is also natural to attribute the broad wings ($10\ \text{cm}^{-1}<\Delta<800\ \text{cm}^{-1}$) of the curves in Fig. 1a to the Δ-independent nonresonant component in (29). Its complex amplitude $\chi_{nr}^{(3)}=\chi_{nr}^0 e^{i\Psi_{nr}}$ was also an adjustable parameter.

The approximation was done as follows. For $\Delta>100$ cm^{-1}, the contribution of χ_{ac} to (29) could be ignored, and this made it possible to determine χ_{nr} on the basis of agreement between the calculated dependence and the data of the experiment for $L=30$ nm. We found χ_{ac} from the different experimental dependence for $L=6$ nm in the region $\Delta<100$ cm^{-1}. Here the experimental data for $L=18$ nm played the role of control data. The calculated dependences $|\chi^{(3)}|^2(\Delta)$ for $\chi_{ac}^0=10$, $\Psi_{ac}=0.72\pi$, $\chi_{nr}^0=2.2$, $\Psi_{nr}=0.95\pi$ are shown in Fig. 1b. It is easy to see that there is excellent qualitative agreement between the results of the calculation and the data of the experiment.

6. CONCLUSIONS

So far as we know, the present model is the first in which allowance has been made in a problem as complicated as four-photon spectroscopy for the real band structure of the investigated object, the locality of its properties in the Brillouin zone, the most important relaxation processes, the saturation of the electron transitions, etc. At the same time, the parameter values and the system of approximations employed are fairly general and make it possible to employ the model to calculate the nonlinear electronic susceptibility in a large class of problems of nonlinear spectroscopy of condensed media. Despite the complexity and apparent abundance of adjustable parameters, the calculation was maximally adapted to a numerical experiment. Fitting of its results was done only through the complex amplitudes of the resonant phonon, the nonresonant parts of the nonlinear susceptibility, and the interband polarization dephasing time. Moreover, for the latter we were able to obtain the extremely important lower bound $T_2 \geqslant 300$ fs. Another very important conclusion is that the saturation effect, which is rather difficult to take into account in practice, can lead only to a change in the efficiency of the nonlinear process without changing the nature of the dispersion dependences.

We have been able to show that the method of biharmonic pumping is very effective in investigations of the electronic spectra of quantum-well structures, including narrow-

band semiconductors. Although the possibility of Raman excitation of optical phonons would seem, at the first glance, to do nothing but make the analysis of the experimental data more difficult, in reality it leads to a significant increase in the amount of spectroscopic information that is obtained. Therefore, the use of the method of biharmonic pumping in conjunction with other methods of investigation must provide a possibility for establishing correspondence between the data obtained by means of them and greatly improve their reliability.

We are sincerely grateful to B. A. Grishanin for his interest and for helpful discussions, and also to V. A. Lobastov for assistance in preparing the experiments.

This work was initiated with financial support by the American Physical Society (Sloan Foundation Grant) and was then continued with financial support by the International Science Foundation (Grant No. RIP000), the Russian Foundation for Fundamental Research (Grant No. 95-02-03639-a), and the State Program "Fundamental Metrology" of the Russian Federation (Project No. 2.68).

[1] Yu. F. Komnik, *Physics of Metallic Films* [in Russian], Atomizdat, Moscow (1979).
[2] R. C. Jaklevic and L. Lambe, Phys. Rev. B **12**, 4146 (1975).
[3] J. Ferre, J. Penissard, C. Marliere *et al.*, Appl. Phys. Lett. **56**, 1588 (1990).
[4] F. J. Himpsel, Phys. Rev. B **44**, 5966 (1991).
[5] D. A. Evans, M. Alonso, R. Cimino, and K. Horn, Phys. Rev. Lett. **70**, 3483 (1993).
[6] B. A. Tavger and V. Ya. Demikhovskiĭ, Usp. Fiz. Nauk **96**, 61 (1968) [Sov. Phys. Usp. **11**, 644 (1970)].
[7] S. S. Nedorezov, Fiz. Tverd. Tela (Leningrad) **12**, 2269 (1970) [Sov. Phys. Solid State **12**, 1814 (1970)].
[8] Yu. F. Ogrin, V. N. Lutskiĭ, and M. I. Elinson, Pis'ma Zh. Eksp. Teor. Fiz. **3**, 114 (1966) [JETP Lett. **3**, 71 (1966)].
[9] V. N. Lutskiĭ, D. N. Korneev, and M. I. Elinson, Pis'ma Zh. Eksp. Teor. Fiz. **4**, 267 (1966) [JETP Lett. **4**, 179 (1966)].
[10] L. L. Chang, in *Highlights in Condensed Matter: Physics and Future Prospects*, Plenum, New York (1991).
[11] *Quantum Well and Superlattice Physics*, Proc. SPIE **943**, (1988).
[12] B. A. Grishanin, V. M. Petnikova, and V. V. Shuvalov, in *Reviews of Science and Technology. Modern Problems of Laser Physics*, Vol. 2 [in Russian], VINITI, Moscow (1990).
[13] A. N. Zherikhin, V. A. Lobastov, V. M. Petnikova, and V. V. Shuvalov, Phys. Lett. A **179**, 145 (1993).
[14] A. N. Zherikhin, in *Reviews of Science and Technology. Modern Problems of Laser Physics*, Vol. 1 [in Russian], VINITI, Moscow (1990).
[15] R. Dalven, Infrared Phys. **9**, 141 (1969).
[16] Yu. I. Ravich, B. A. Efimova, and I. A. Smirnov, *Methods of Investigating Semiconductors as Applied to the Lead Chalcogenides PbTe, PbSe, PbS* [in Russian], Nauka, Moscow (1968).
[17] M. Cardona and D. L. Greenaway, Phys. Rev. **133**, 1685 (1964).
[18] Landolt-Bornstein, *Numerical Data and Functional Relationships in Science and Technology*, Group III, **17f**, 170, Springer, Berlin (1983).
[19] J. A. Reissland, *The Physics of Phonons*, Wiley, New York (1973).
[20] B. A. Grishanin, V. A. Lobastov, V. M. Petnikova, and V. V. Shuvalov, Laser Physics **3**, 121 (1993).
[21] P. J. Lin and L. Kleinman, Phys. Rev. **142**, 478 (1966).
[22] L. N. Vereshagina, A. N. Zherikhin, A. G. Kornienko *et al.*, Kvantovaya Elektron. (Moscow) **21**, 855 (1994) [*sic*].
[23] K. Tanaka, H. Olitake, and T. Snemoto, Phys. Rev. Lett. **71**, 1935 (1993).
[24] J. Christen and D. Bimberg, Surf. Sci. **174**, 261 (1986).
[25] J. M. Ziman, *Principles of the Theory of Solids*, 2nd ed., Cambridge University Press, London (1972).
[26] P. A. Apanasevich, *Fundamentals of the Theory of the Interaction of Light with Matter* [in Russian], Nauka i Tekhnika, Minsk (1977).

Translated by Julian B. Barbour